frontiers | Frontiers in Nuclear Engineering

TYPE Original Research
PUBLISHED 13 December 2023
DOI 10.3389/fnuen.2023.1306529

OPEN ACCESS

EDITED BY
Anne Campbell,
Oak Ridge National Laboratory (DOE),
United States

REVIEWED BY
Shingo Tamaki,
Osaka University, Japan
Karim Ahmed,
Texas A&M University, United States
Elizabeth Sooby,
University of Texas at San Antonio,
United States

*CORRESPONDENCE
Janelle P. Wharry,
jwharry@purdue.edu

RECEIVED 04 October 2023
ACCEPTED 27 November 2023
PUBLISHED 13 December 2023

CITATION
Wharry JP, Guillen DP, Clement CD, Bin Habib S, Jiang W, Zhao Y, Lu Y, Wu Y, Shiau C-H, Frazer D, Heidrich BJ, Knight C and Gandy DW (2023), Materials qualification through the Nuclear Science User Facilities (NSUF): a case study on irradiated PM-HIP structural alloys. *Front. Nucl. Eng.* 2:1306529. doi: 10.3389/fnuen.2023.1306529

Materials qualification through the Nuclear Science User Facilities (NSUF): a case study on irradiated PM-HIP structural alloys

Janelle P. Wharry[1]*, Donna Post Guillen[2], Caleb D. Clement[1,3], Saquib Bin Habib[1], Wen Jiang[1], Yangyang Zhao[1], Yu Lu[4,5], Yaqiao Wu[4,5], Ching-Heng Shiau[4,5], David Frazer[2], Brenden J. Heidrich[2], Collin Knight[2] and David W. Gandy[6]

[1]School of Materials Engineering, Purdue University, West Lafayette, IN, United States, [2]Idaho National Laboratory, Idaho Falls, ID, United States, [3]Westinghouse Electric Company, LLC, Pittsburgh, PA, United States, [4]Micron School of Materials Science and Engineering, Boise State University, Boise, ID, United States, [5]Center for Advanced Energy Studies, Idaho Falls, ID, United States, [6]Electric Power Research Institute, Charlotte, NC, United States

This article presents neutron irradiation and post-irradiation examination (PIE) capabilities available to the nuclear materials research community through the US Department of Energy's Nuclear Science User Facilities (NSUF). The pressing need to deploy advanced nuclear reactors to combat climate change requires qualification of new fuels and materials. Among advanced manufacturing processes, powder metallurgy with hot isostatic pressing (PM-HIP) is nearest to becoming qualified for nuclear applications. This article provides examples from a recent irradiation and PIE program on a series of structural alloys fabricated by PM-HIP to illustrate how NSUF capabilities can be used to generate qualification data. The neutron irradiation experiments are described, and a sampling of results from tensile testing, nanoindentation, transmission electron microscopy, and atom probe tomography are presented, showing the favorable performance of PM-HIP alloys compared to their cast or forged counterparts under irradiation. This article provides a perspective on leveraging NSUF for future nuclear fuels and materials testing and qualification.

KEYWORDS

materials qualification, neutron irradiation, powder metallurgy, mechanical testing, irradiated microstructure, user facility, hot isostatic pressing, structural alloys

1 Introduction

Materials development and qualification for the nuclear power industry have historically been protracted processes by comparison to other industries (Olson and Kuehmann, 2014), in large part due to the need to evaluate the in-reactor performance of materials (Aguiar et al., 2020). Large-scale neutron irradiation and post-irradiation examination (PIE) programs, often termed "campaigns", are the established norms for obtaining irradiation effects and performance data under service-relevant conditions (Crawford et al., 2007; Petti et al., 2010), which can subsequently be used toward materials qualification. Often, sequential campaigns are necessary to take advantage of an iterative materials design cycle. Each campaign can often span a decade and cost multiple millions of US dollars. Consequently, qualification of new materials has long been a bottleneck for the nuclear power industry, and the list of "qualified"

materials is mostly limited to those in use since the earliest commercial nuclear power plants in the late 1950s.

Currently qualified nuclear materials will not suffice for advanced reactor designs—the deployment of which is increasingly crucial to combating climate change (Sailor et al., 2000; Chu and Majumdar, 2012; Mathew, 2022). Many of these advanced reactor designs demand materials to operate at higher temperatures, higher irradiation fluences, and in more corrosive environments compared to current light water reactors (LWRs). The recent boon in advanced manufacturing (Kautz et al., 2019; Blevins and Yang, 2020; Morgan et al., 2022) and data-driven, machine learning–based materials design (Stach et al., 2021) has introduced a tremendous breadth of innovative nuclear fuel and material concepts, novel manufacturing methods for established materials, and advanced welding and joining techniques, which show promise for advanced reactors. To bring these materials and methods full circle in an advanced reactor therefore requires a transformation in our capabilities to qualify new nuclear materials.

Wide-ranging efforts to accelerate nuclear fuels and materials qualification are being pursued across the research community (Murty and Charit, 2008; Gong et al., 2016; Aguiar et al., 2020). For example, automation is being used to modularize nuclear manufacturing (Kautz et al., 2019; Blevins and Yang, 2020; Morgan et al., 2022), coupled with *in situ* process monitoring to accelerate and simplify quality assurance of advanced manufactured components (Everton et al., 2016; Sun et al., 2021). High-throughput experiments, separate effects, and small-scale mechanical testing are being developed to improve and accelerate materials screening and downselection before investing in neutron irradiation and PIE campaigns (Terrani et al., 2020; Hensley et al., 2021; Moorehead et al., 2021). Data analytics and machine learning are being leveraged to improve predictive capabilities of modeling tools to maximize the return on investment in irradiation testing (Stach et al., 2021; Morgan et al., 2022).

As irradiation testing remains a cornerstone of nuclear materials qualification, assessing our capacity to conduct these critical experiments will provide the community with a guide for efficient materials qualification campaigns. This article presents irradiation and PIE campaign capabilities within the United States, available through direct and competitive funding from the Department of Energy, Office of Nuclear Energy, Nuclear Science User Facilities (NSUF). An irradiation and PIE campaign on structural alloys fabricated by powder metallurgy with hot isostatic pressing (PM-HIP) is used as an example throughout the article. An overview of results from the campaign are presented to illustrate how NSUF capabilities can be utilized to generate qualification datasets. The article concludes with a perspective on the use of NSUF for future materials testing and qualification efforts.

PM-HIP alloys are the ideal set of materials for this article because among advanced manufacturing technologies, PM-HIP is closest to becoming fully qualified for nuclear applications (Gandy et al., 2019). The nuclear industry is seeking to replace traditional castings or forgings with PM-HIP manufacturing for LWR (Gandy et al., 2012; Gandy et al., 2019) and small modular reactor (SMR) (Gandy et al., 2019) internals, pressure vessels (Morrison et al., 2019), and secondary side components. PM-HIP offers numerous advantages over conventional alloy fabrication, including an equiaxed, fine-grained structure (Clement et al., 2022a; Clement et al., 2022b), chemical homogeneity (Yu et al., 2009; Ahmed et al., 2013; Shulga, 2013; Ahmed et al., 2014; Gandy et al., 2016), exceptional mechanical properties (Metals and and Ceramics Information Center Report No, 1977; Atkinson and Davies, 2000; Rao et al., 2003; Shulga, 2012; Shulga, 2014; Guillen et al., 2018; Morrison et al., 2019; Barros et al., 2022) especially at high temperatures (Bullens et al., 2018; Getto et al., 2019), greater irradiation resistance (van Osch et al., 1996; Lind and Bergenlid, 2000; Rodchenkov et al., 2000; Lind and Bergenlid, 2001; Clement et al., 2022a; Clement et al., 2022b), fewer defects (Gandy et al., 2012; Gandy et al., 2019), and near-net–shaped fabrication which reduces reliance on welding and machining (Mao K. S. et al., 2018; Mao K. et al., 2018; Mao et al., 2021). PM-HIP-manufactured ferritic steels, austenitic steels, and Ni-based alloys are already qualified for non-nuclear applications, alongside castings and forgings, in the ASME Boiler and Pressure Vessel Code (BPVC), Section 2. More recently, the PM-HIP form of austenitic stainless steel 316 L has been qualified for non-irradiation–facing nuclear applications through ASME BPVC, Section 3. The selected results presented herein can expand PM-HIP qualification for irradiation-facing components and for additional alloys.

2 The NSUF program

The NSUF is one of a diverse group of US Department of Energy (DOE) user facilities. It is the DOE Office of Nuclear Energy's (DOE-NE) first and only sponsored user facility and is singularly focused on advancing technologies supporting nuclear energy applications. The NSUF is unique in that it is not formed from a single self-contained facility but is a consortium of facilities distributed across the nation at 21 institutions. The NSUF is centered at and managed from Idaho National Laboratory (INL) where it was originally founded. The partner facilities include twelve universities, seven national laboratories (in addition to INL), and one industry institute as well as the Center for Advanced Energy Studies (CAES) in Idaho Falls, ID. NSUF also has several active international collaborations that leverage capabilities around the world.

The NSUF has one goal: to produce the highest quality research results that will impact and increase the understanding of nuclear energy technologies important to DOE-NE. The NSUF does not have an objective to develop or qualify a particular type of fuel or structural material, but instead, the NSUF performs research projects related to all areas of irradiation effects in nuclear fuels and materials that will increase the knowledge and understanding associated with phenomena or behaviors that will have an impact on advancing nuclear technology. By acting as a user facility and providing the user with no-cost access to its specialized and unique capabilities, the NSUF program fosters the development of novel ideas generated by external contributors from universities, national laboratories, and industry while promoting collaborations between those contributors and the expertise associated with the NSUF partner capabilities. These collaborations define the cutting edge of nuclear technology research in understanding the behavior of materials subjected to radiation environments, contribute to improved performance of current industry and future nuclear reactor systems, and stimulate cooperative research between user groups conducting research in nuclear energy systems.

The NSUF is comprised of many complementary, interrelated components that are fully engaged in building sustainable value over the long term. It delivers high impact results through its outstanding program support staff and partners, its unique facilities, and its unrivaled capabilities. The NSUF seeks to offer the broadest and most advanced technologies to the nuclear research community. The institutions that host the facilities that make up the NSUF offer capabilities that span the entire scope of requirements needed for in-depth nuclear fuels and materials irradiation testing. The capabilities of the NSUF, in conjunction with institutional expertise, can accommodate the simplest to the most complex projects that might require design, fabrication, transportation, irradiation, post-irradiation examination (including advanced materials science characterization), and final disposition. Thus, the NSUF offers nuclear test and research reactor facilities including associated neutronic and thermal hydraulic support calculations, ion irradiation facilities, radiation-qualified fabrication facilities, hot cell capabilities, high-level radiation shielded instrumentation, and low-level radiation instrumentation as well as high performance computing (HPC) and access to neutron, positron, and synchrotron X-ray beam line capabilities.

In addition to physical capabilities and personnel expertise, the NSUF maintains digital resources to support nuclear energy research and researchers. The NSUF developed three databases that can be accessed at the NSUF website: one for nuclear energy associated research and development capabilities known as the Nuclear Energy Infrastructure Database (NEID); one for collaboration, the Nuclear Energy Researcher Database (NERD); and one for nuclear materials available for use by investigators in nuclear energy research projects known as the Nuclear Fuels and Materials Library (NFML). The physical half of the NFML contains specimens of irradiated and unirradiated nuclear fuel and material covering a wide range of material types from past and ongoing irradiation test campaigns, legacy components obtained from decommissioned power reactors, and donations from other laboratories. The NFML is intended to enable time and cost savings by reducing the number of irradiation tests that must be performed to generate material performance data.

Finally, the NSUF, with support from the INL High Performance Computing (HPC) team have developed the Nuclear Research Data System (NRDS). NRDS is intended to store all NSUF project data, available only to the research team during the performance of the awarded work and then open to the public to fuel collaboration and to accelerate the deployment of advanced nuclear energy technologies. NSUF partner facilities and researchers can upload the data and assign one of 20 licenses to guide how it will be used in the future and what attribution is required. NRDS data sets are available from the NSUF and INL HPC websites but will also have individual DOI numbers and will be indexed by major search engines for global accessibility. Since this data is located within the HPC infrastructure at INL, researchers can perform a wide variety of built-in and custom artificial intelligence/machine learning, data processing, and visualization activities without the need to locally download these large data sets.

NSUF was founded in 2007 with one reactor and one hot cell facility. The program continues to grow and adapt to changing national priorities and researcher needs. The program office works with DOE-NE, the US nuclear industry, other user facilities, and its own researchers to inform its operations and growth. While the primary focus of NSUF will always be on nuclear fuels and materials, other areas of endeavor are possible. NSUF works to maintain flexibility and adaptability to the needs of the US nuclear energy community.

3 Methods and materials

3.1 Neutron irradiation

NSUF offers several test reactors for fuels and materials irradiation campaigns, including the Advanced Test Reactor (ATR) at INL, Transient Reactor Test (TREAT) Facility at INL, the High Flux Isotope Reactor (HFIR) at Oak Ridge National Laboratory (ORNL), the Massachusetts Institute of Technology (MIT) Reactor, and the North Carolina State University PULSTAR Reactor. Each of these reactors offers a unique range of fluxes, neutron spectra, and instrumented and controlled testing options, suitable for a wide variety of fuels and materials testing and qualification. For this project, ATR was selected for its relatively high thermal neutron flux (relative to fast flux) and lower temperature capabilities, both of which are more representative of the LWR environments in which the studied alloys are intended to operate. Additionally, ATR offers relatively large test volumes, able to accommodate specimen geometries such as ASTM E8 standardized tensile bars for materials qualification efforts.

For the case study highlighted here, we examined steel and nickel-based alloys intended for nuclear reactor applications. Six structural alloys are included in the irradiation campaign, each fabricated by PM-HIP and by either forging or casting. The alloys were SA508 Grade 3 Class 1 low-alloy RPV steel, Ni-based Alloys 625 and 690, Grade 91 ferritic steel, and austenitic stainless steels 316L and 304 L. The alloys were compliant with ASME BPVC compositional specifications, and were all provided by the Electric Power Research Institute. For all alloys, HIP was conducted at a pressure of 15 ksi for 4 h; HIP temperature was 1149°C for the two Ni-based alloys or 1121°C for all other alloys. The heat treatments for the HIP and cast/forged materials followed standard heat treatment procedures for the specific alloys. The two Ni-based alloys and the two austenitic stainless steels were solution cycled then water quenched; the Grade 91 was normalized and tempered; and the SA508 was solution cycled, quenched, normalized, and tempered. Specimen geometries were ASTM E8 round tensile bars for mechanical property evaluation, transmission electron microscopy (TEM) discs (i.e., coupons) for microstructure characterization and nanoindentation, and pre-cracked miniature compact tension (CT) specimens for fracture toughness testing. More comprehensive description of the alloy compositions, fabrication and heat treatment details, and specimen machining methods are described in ref. (Guillen et al., 2023).

3.2 Mechanical testing

Uniaxial tensile testing of radioactive specimens was conducted using a 13 M Instron load cell in the hot cells at the Hot Fuel Examination Facility (HFEF) at INL. Testing was conducted at

ambient temperature in an argon environment following ASTM E8 for threaded grip specimens. The load capacity of the cell was 50 kN, and loading rate range was 0.001 mm/min-500 mm/min. In the present experiments, a strain rate of 8.78×10^{-3} s^{-1} (0.279 mm/min crosshead speed) was used through 10% strain, after which the strain rate increased to 3.15×10^{-2} s^{-1} (1.0 mm/min crosshead speed) until failure. Time, load, and displacement were recorded throughout the test, and have been archived in (Wharry et al., 2023). After tensile testing, fracture surfaces were cut from the broken tensile halves using a diamond wafering blade; this enabled the fracture surfaces to be oriented face-up in a scanning electron microscope (SEM) for fractography. A Lyra3 Tescan SEM at the Electron Microscopy Laboratory (EML) at INL was used for fracture surface characterization. Fractographs are also archived in (Wharry et al., 2023).

Nanoindentation hardness measurement capabilities on the Hysitron TI-950 TriboIndenter are available through NSUF at the Microscopy and Characterization Suite (MaCS), CAES. Nanoindentation is used to rapidly evaluate hardness and elastic modulus, especially in irradiation campaigns that are unable to accommodate ASTM standard-sized tensile bars or for volume-limited specimens (Chen et al., 2020). The TI-950 can be operated with a Berkovich tip in depth-controlled or load-controlled mode, with a maximum load of 2.2 N. In the present work, nanoindentation was conducted in depth-controlled mode to a maximum depth of 3,500 nm at a strain rate of 0.2 s^{-1}. The displacement and load were recorded continuously as a function of time, from which the nanoindentation hardness was calculated using the Oliver-Pharr method (Oliver and Pharr, 2004).

3.3 Microstructure characterization

NSUF has several dedicated radioactive TEM capabilities, including the FEI (now ThermoFisher) Tecnai TF30-FEG STwin TEM at MaCS, CAES, used in this project. The instrument is equipped with energy dispersive x-ray spectroscopy (EDS), electron energy loss spectroscopy (EELS), energy filtered TEM (EFTEM), scanning TEM (STEM), and TopSpin. The instrument has been used across numerous NSUF projects to characterize irradiation-induced defects, including dislocation loops using techniques including two-beam condition (rel-rod) imaging or down-zone STEM (Parish et al., 2015), voids or bubbles using the through-focus technique, phase evolution using diffraction and EDS, and nanoclustering and radiation-induced segregation using EDS line and area mapping. To evaluate the performance of PM-HIP alloys, TEM characterization focused on precipitate and dislocation loop evolution under irradiation. In this work, the TEM was operated in scanning TEM (STEM) mode at 200 kV. STEM high-angle annular dark field (HAADF) imaging was used to observe the precipitate number density and distribution, with high resolution STEM to observe the precipitate structures. Bright-field down-zone STEM imaging was used to observe dislocation loops, following a technique described in (Parish et al., 2015).

Atom probe tomography: NSUF offers capabilities for three-dimensional (3D) atomic-scale chemical characterization using the CAMECA Local Electrode Atom Probe (LEAP) 4000X HR at MaCS, CAES dedicated for radioactive specimens. Atom probe tomography (APT) utilizes the principle of field evaporation on a ~10–100 nm diameter needle specimen; the evaporated species from the needle are collected in a time-of-flight mass spectrometer, enabling atom-by-atom position-sensitive 3D reconstruction of the needles. The LEAP 4000X HR at CAES is capable of laser or voltage pulsing with 250 kHz laser or 200 kHz voltage pulse generator. Metallic specimens can often be analyzed using voltage pulsing for high mass resolution; however, specimens having limited conductivity must be analyzed using laser pulsing, which may limit mass resolution (Sen et al., 2021). In the current work, specimens were tested in laser pulse mode with 60 pJ laser energy, 200 kHz pulse rate, and specimen base temperature ~50 K. APT raw data files were reconstructed using the CAMECA proprietary AP Suite software, with cluster analysis conducted following established procedures (Vaumousse et al., 2003; Hyde et al., 2011; Williams et al., 2013; Swenson and Wharry, 2015; Swenson and Wharry, 2016).

4 Results demonstration

4.1 Neutron irradiation

Irradiation capsules, fixtures, and loading schemes were designed such that each PM-HIP specimen and its cast or forged counterpart would receive consistent fluences and temperatures, enabling a direct comparison of microstructure and mechanical property evolution across fabrication methods. A total of 256 specimens, including 48 round tensile bars, 28 miniature CTs, and 180 TEM discs, were irradiated in a set of seven non-instrumented, drop-in capsules. Melt wires were inserted into the center fixtures of each capsule. Capsules were stacked vertically, with complete loading configurations described in ref. (Guillen et al., 2023). Neutron physics, thermal, and structural analyses were conducted during the design phase to ensure proper fluence and temperature requirements were met for all specimens within this stacked configuration. Details of these calculations are provided in refs. (Brookman, 2018; Hale, 2018). and summarized in ref. (Guillen et al., 2023).

The capsules were inserted for irradiation to the inboard A6, A7, and A8 positions during ATR cycles 164A, 164B, 166 A and 166B, spanning May 2018 through January 2020. Fluxes ranged 8.08–9.61 × 10^{14} neutrons/cm^2·s, with fast (>1 MeV) flux components ranging 1.60–1.96 × 10^{14} neutrons/cm^2·s. As-run fluences (Brookman, 2020) and temperatures (Davis and Hone, 2020; Hale, 2021) are tabulated for each specimen in ref. (Guillen et al., 2023). Actual doses ranged 0.5–1.1 dpa and 2.7–5.4 dpa for the dose targets of 1 and 3 dpa, respectively, corresponding to a dose rate range of 1.0–1.8 10^{-7} dpa/s. Finite element analysis (FEA) based thermal analysis determined actual temperature ranges of 257°C–306°C and 321°C–398°C for the temperature targets of 300°C and 400°C, respectively.

4.2 Uniaxial tensile testing & fractography

As an example, we consider the tensile testing results from neutron irradiated cast and PM-HIP 316 L stainless steel, Figure 1A. The two PM-HIP specimens have irradiation conditions of 3.91 dpa

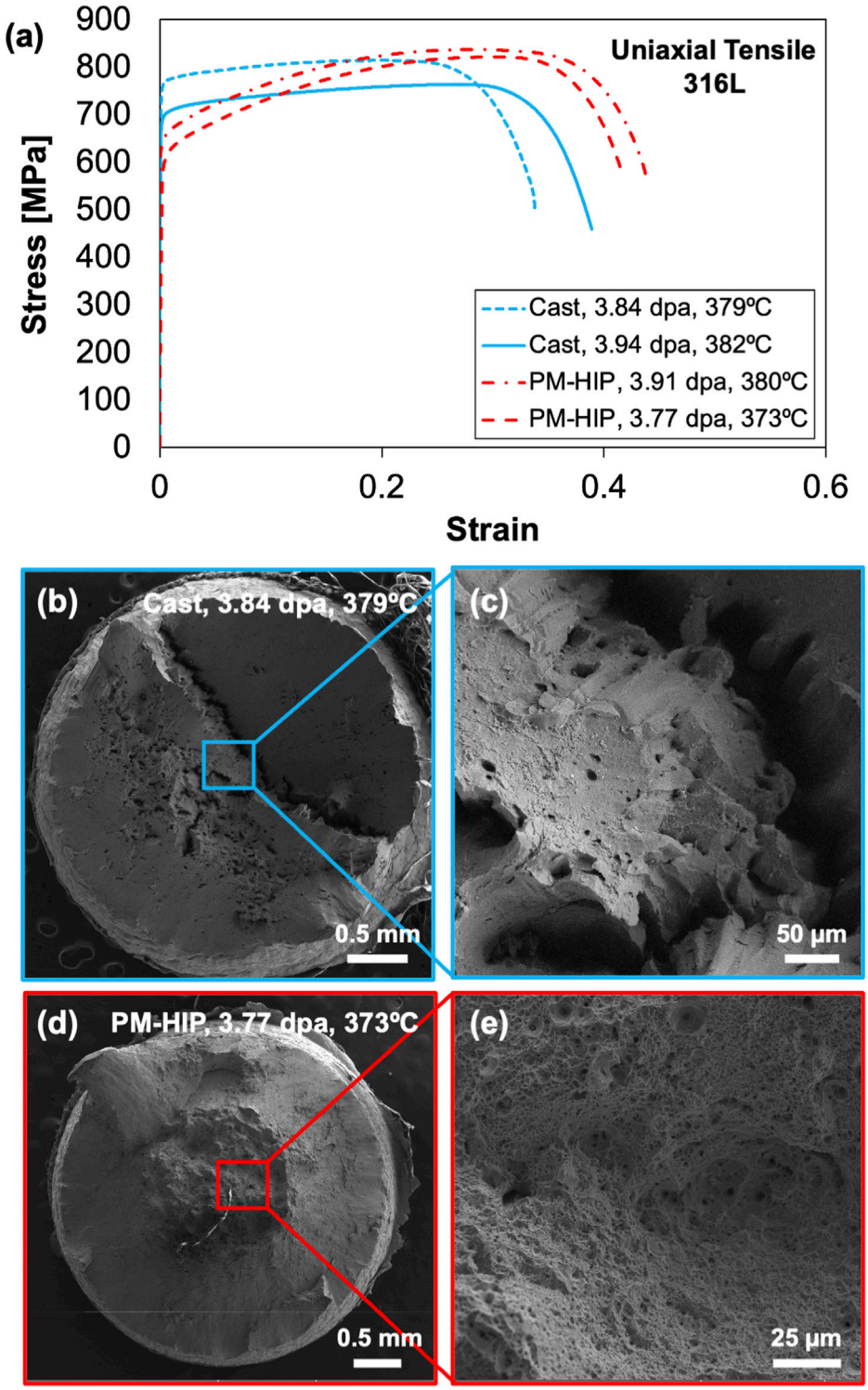

FIGURE 1
Example uniaxial tensile results from cast and PM-HIP 316 L stainless steel, neutron irradiated to nominally 3.8–3.9 dpa at ~370°C–380°C, showing **(A)** stress-strain curves, and SEM fractography of irradiated **(B,C)** cast specimen and **(D,E)** PM-HIP specimen. Micrographs **(B–E)** adapted from (Wharry et al., 2023), licensed under CC BY 4.0.

at an average irradiation temperature of 380°C (specimen 719) and 3.77 dpa at an average irradiation temperature of 373°C (specimen 720). The two cast specimens have irradiation conditions of 3.84 dpa at an average irradiation temperature of 379°C (specimen 704) and 3.94 dpa at an average irradiation temperature of 382°C (specimen 705). The specimen identification numbers correspond to descriptions provided in ref. (Guillen et al., 2023). Results show that after irradiation, PM-HIP specimens exhibit ~10–15% greater

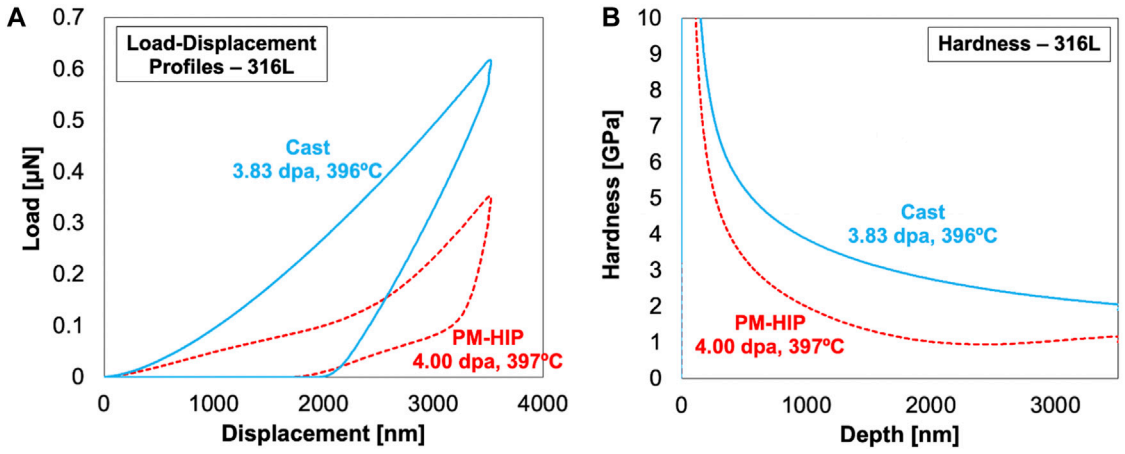

FIGURE 2
Example nanoindentation results from 316 L stainless steel, showing average **(A)** load-displacement curves and **(B)** hardness depth profiles, averaged over 26 indents in cast and PM-HIP specimens irradiated to nominally 3.8–4.0 dpa at ~400°C.

ductility than the cast specimens. Although the irradiated PM-HIP specimens have a lower yield strength than the cast specimens by ~150 MPa, the PM-HIP specimens have greater strain hardening capacity, resulting in a higher ultimate tensile stress (UTS) than the cast specimens. The lower ductility of the cast specimen is evident from fractography, which shows a relative flat fracture surface with possible tearing-type behavior in cast specimen 704 (Figure 1B); by contrast, PM-HIP specimen 720 exhibits a classic ductile cup-cone type fracture surface at low magnifications (Figure 1D). At higher magnification, the PM-HIP fracture surface is heavily dimpled (Figure 1E), providing further contrast to the more brittle, dimple-free cast fracture surface (Figure 1C).

The greater ductility of the PM-HIP specimen may be due to its finer grain structure as compared to the forged specimen. Guillen, et al., (Guillen et al., 2018), used far-field high energy X-ray diffraction (ff-HEDM) *in situ* tensile testing of the unirradiated versions of these exact 316 L PM-HIP and forged materials. They observed the finer PM-HIP grain structure gave rise to a more homogeneous distribution of grain-level stress in the loading direction. This stress homogenization limits the formation of stress concentrations which could lead to more brittle failure. Assuming this stress heterogeneity persists throughout irradiation, the PM-HIP specimen will also be less susceptible to stress concentrations resulting from localized deformation mechanisms that tend to occur in austenitic stainless steels after irradiation (Jiao and Was, 2010; McMurtrey et al., 2011; West et al., 2012; De Bellefon and Van Duysen, 2016; Mao et al., 2020; Wharry and Mao, 2020).

Additionally, in the unirradiated states, the PM-HIP exhibits higher yield strength than the forged specimen (Guillen et al., 2018), explained by the Hall–Petch relationship. However, under irradiation, a finer grain structure provides a high sink density that facilitates recombination of irradiation-induced defects (Odette and Hoelzer, 2010; Yu et al., 2013; Du et al., 2018; Zhang et al., 2018; Patki et al., 2020). Hence, the finer grain structure may make the PM-HIP 316 L more irradiation-tolerant than forged 316L, thus accumulating a lesser extent of irradiation hardening. Future irradiated microstructure examinations will help further rationalize these mechanical behaviors.

4.3 Nanoindentation

Example nanoindentation results are from disc-type specimens of 316 L stainless steel, irradiated to similar conditions as the 316 L tensile bars described in Section 2.2. Specifically, PM-HIP 316 L was irradiated to 4.00 dpa at an average temperature of 397°C (specimen 646), while cast 316 L was irradiated to 3.83 dpa at an average temperature of 396°C (specimen 643). The average nanoindentation load-displacement curves and the corresponding average hardness-depth profiles are shown for both the PM-HIP and cast specimens in Figure 2. Note that the results shown are the average of 26 indents made on each specimen; these load-displacement-time raw datasets are available in (Wharry et al., 2023). The load-displacement curves show that a higher load is required to reach the same indent depth in the cast specimen than in the PM-HIP specimen; correspondingly, the cast material has a higher hardness by ~1.5 GPa. With relatively negligible differences in the actual irradiation dose and temperature between the cast and PM-HIP specimens, the hardness difference is thus likely a true hardness difference that can be ascribed to the material microstructure. This behavior is consistent with the lower yield strength and higher strain hardenability of PM-HIP 316 L observed in uniaxial tension testing (Figure 2B).

4.4 Transmission electron microscopy

Demonstration of TEM work is shown for SA508 Grade 3 Class 1 low-alloy steel in Figure 3. The PM-HIP specimen (431) was irradiated to 0.97 dpa at an average temperature of 388°C, while the forged specimen (437) was irradiated to 0.95 dpa at an average temperature of 384°C. Precipitates in the PM-HIP specimens are spherical and homogeneously dispersed, with average diameter 48 ± 3 nm after irradiation. Meanwhile, precipitates in the forged specimen are needle-like with average length 105 ± 9 nm and appear heterogeneously distributed primarily along grain and subgrain boundaries, with some precipitates located on grain interiors. The PM-HIP precipitates are amorphous, while the

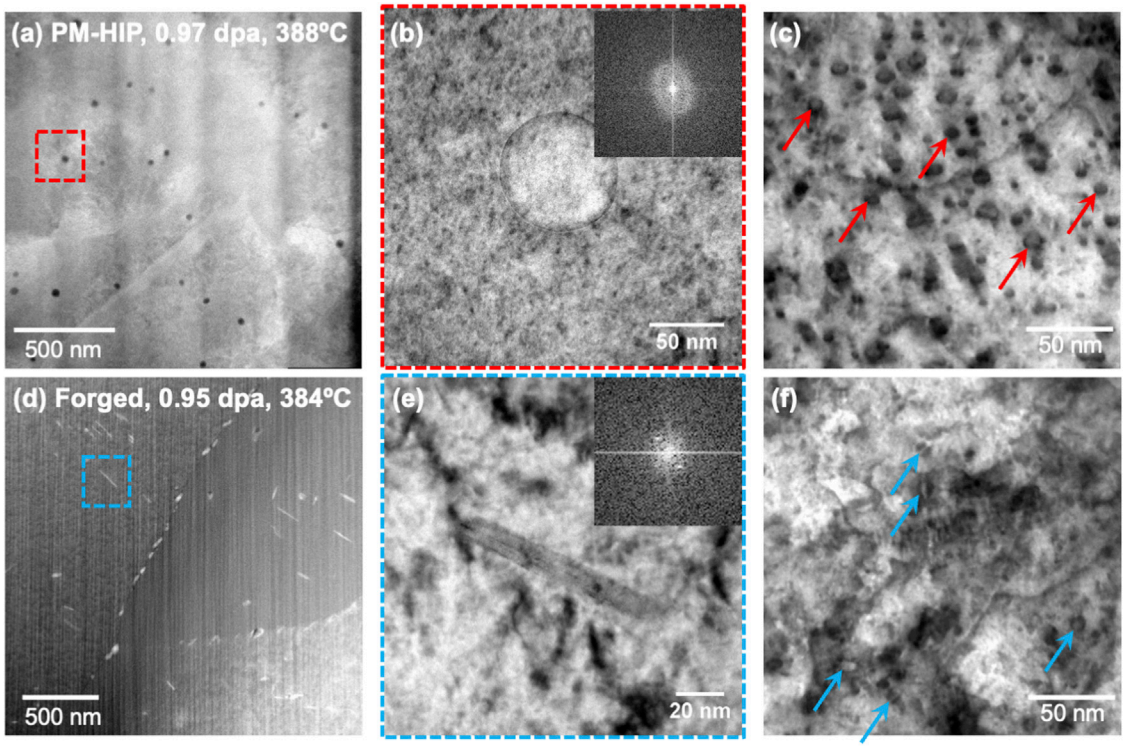

FIGURE 3
TEM micrographs from neutron irradiated SA508 to 0.95–0.98 dpa, 384°C–388°C: **(A–C)** PM-HIP specimen showing **(A)** precipitate distribution, with selected precipitate at higher magnification in **(B)** with inset diffraction pattern suggesting amorphous structure, and **(C)** arrowed dislocation loops; and **(D–F)** Forged specimen showing **(D)** precipitate distribution, with selected precipitate at higher magnification in **(E)** with inset diffraction pattern suggesting semi-crystalline structure, and **(F)** arrowed dislocation loops.

forged precipitates appear at least semi-crystalline given their diffraction spots. Dislocation loops are smaller but more populous in the PM-HIP material than in the forged, suggesting the overall susceptibility to dislocation-type defects may be somewhat comparable between the two fabrication methods.

Differences in the irradiation evolution of the precipitates may be ascribed to their compositions and initial crystal structure. As proposed by Motta (Motta, 1997), irradiation-induced amorphization requires that the change in configurational entropy exceeds the change in enthalpy. This entropy increase can be attained by relaxation of long-range order requirements, consequently leading to an abrupt increase in the available short-range order configurations. Needle-like and preferentially oriented precipitates such as those in the forged material, tend to be incoherent with the matrix, whereas randomly distributed round precipitates such as those in the PM-HIP material, tend to be coherent (Zain-ul-abdein and Nélias, 2016). Since incoherency is associated with higher residual stresses, this may translate to a greater amount of stored mechanical energy in the round PM-HIP precipitates. This greater stored energy contributes to the total entropy required to induce amorphization, effectively making it easier to amorphize the PM-HIP precipitates.

The greater dislocation loop density in the PM-HIP alloy may be due to its chemical composition. In RPV steels at doses above ~0.1 dpa, irradiation drives Mn-Ni-Si (MNS) or Mn-Ni-Si-P (MNSP) nanoclusters to agglomerate on point defect clusters (Meslin et al., 2010; Bonny et al., 2013; Bonny et al., 2014). This muddles the distinction between nanoclusters and defect clusters, the latter of which grow into dislocation loops at higher fluences (Maussner et al., 1999; Kočık et al., 2002; Kuleshova et al., 2002; Gurovich et al., 2009; Meslin et al., 2010). Once these loops become large enough to be resolved in TEM, they are often decorated by Mn and Ni (and Cu, if present in the bulk material) (Fujii et al., 2005; Hamaoka et al., 2010). This underscores the importance of Mn and Ni in stabilizing the loop and nanoprecipitate population. The higher bulk concentration of Mn and Ni in the PM-HIP alloy (1.39 wt% and 0.79 wt%, respectively) than in the forged alloy (0.46 wt% Mn and 0.50 wt% Ni) can explain the higher loop number densities in the PM-HIP alloy. This finding suggests that irradiation susceptibility of RPV steels may be more strongly influenced by bulk alloy chemistry than processing method.

4.5 Atom probe tomography

APT is demonstrated on Grade 91 ferritic steel in Figure 4. Both the PM-HIP and cast specimens were irradiated to 0.99 dpa (specimens 424 and 425) at an average temperature of 389°C. Two

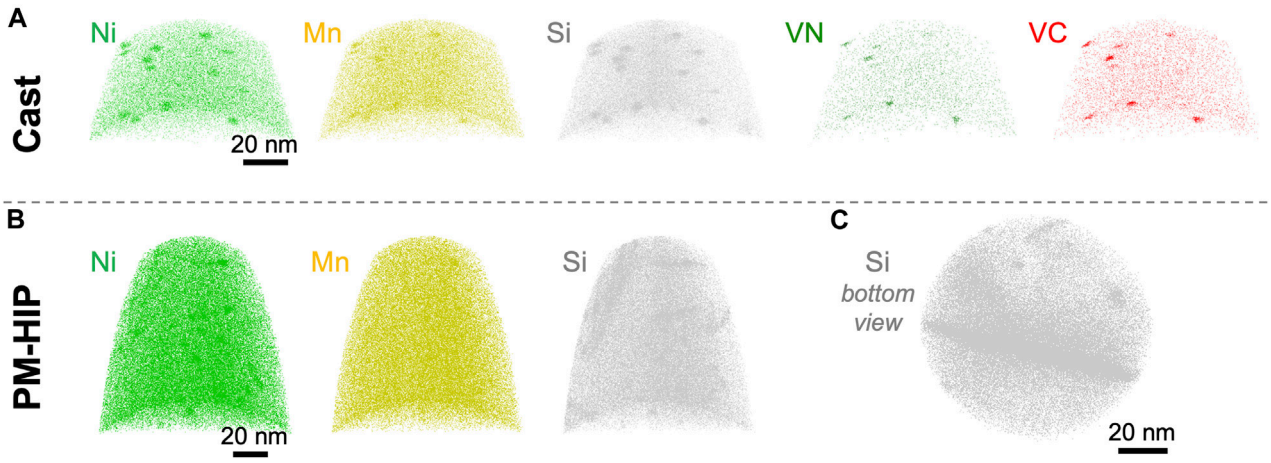

FIGURE 4
APT reconstructions from ~1 dpa, 389°C neutron irradiated Grade 91, showing **(A)** cast specimen with Ni, Mn, Si, VN, and VC nanoclusters, **(B)** PM-HIP specimen with Ni, Mn, and Si nanoclusters with **(C)** Si segregation to dislocation lines.

TABLE 1 Quantitative APT analysis of multiple tips taken from cast and PM-HIP Grade 91 steel, following neutron irradiation to ~1 dpa at 389°C.

Alloy (clustered species)	Tip number	Cluster radius (nm)	Number density (10^{22} m^{-3})	Volume fraction (%)
Cast (Ni, Mn, Si, VN, VC)	1	2.48	5.53	0.41
	2	2.03	4.16	0.16
	Average	2.26 ± 0.32	4.84 ± 0.97	0.28 ± 0.18
PM-HIP (Ni, Mn, Si)	1	1.46	3.06	0.06
	2	1.59	7.58	0.04
	3	1.82	4.66	0.22
	4	1.76	7.17	0.06
	5	2.38	2.00	0.43
	Average	1.80 ± 0.35	4.89 ± 2.46	0.16 ± 0.17

needles were analyzed from the cast specimen, and five from the PM-HIP specimen (Table 1). Qualitatively, representative reconstructions of the analyzed needles show a distribution of fine Ni-Mn-Si nanoclusters in both the cast and PM-HIP specimens (Figures 4A, B). However, nanoclusters in the cast specimen also contain Vanadium Nitride (VN) and Vanadiaum Carbide (VC) molecules, while those in the PM-HIP specimen do not. Additionally, the PM-HIP specimen appears to exhibit Suzuki-like segregation of the clustering species to dislocation features, particularly Si (Figure 4C). Quantitatively, the PM-HIP and cast nanoclusters are statistically identical (Table 1), although the PM-HIP has slightly smaller nanocluster diameters and volume fractions than the cast specimen. The PM-HIP to cast comparison of nanocluster compositions and sizes is somewhat surprising, given that the PM-HIP has a higher bulk Ni, Mn, Si, and V concentration (Wharry et al., 2023). This may suggest that the PM-HIP specimen is inherently resistant to irradiation-induced chemical segregation and redistribution, though the cause has not yet been identified. Alternatively, solute segregation to dislocations in the PM-HIP material may leave few solute atoms available for nucleating nanoclusters. Further microstructure investigation of Grade 91, including at higher irradiation doses, may shed light on the greater resistance of PM-HIP to nanocluster nucleation.

5 Summary and perspective

This work demonstrates the use of a wide range of NSUF capabilities to generate neutron irradiation performance data on nuclear structural materials, through a comprehensive irradiation and post-irradiation examination campaign. The overall irradiation campaign is designed to enable a systematic comparison of mechanical and microstructural evolution between the PM-HIP and cast/forged variants; selected materials and irradiation conditions are shown as four examples herein:

TABLE 2 Summary of irradiation performance of PM-HIP materials compared to their cast or forged counterparts on the basis of mechanical properties and microstructure evolution (favorable = PM-HIP performs better than cast/forged).

Alloy	Mechanical properties	Microstructure evolution	References
Alloy 625	Favorable	Comparable	Clement et al. (2022b)
Alloy 690	Favorable	Comparable	unpublished
Grade 91	Comparable	Comparable	Wharry et al. (2023), this work
SA508	Unfavorable	Unfavorable	Jiang et al. (2023)
316 L	Favorable	TBD	Wharry et al. (2023), this work
304 L	N/A	N/A	N/A

1. Uniaxial tensile testing and fractography reveals that at ~3.8–3.9 dpa at ~370°C–380°C, PM-HIP 316 L stainless steel exhibits lower yield strength, greater ductility, and greater strain hardening capacity than cast 316 L.
2. Nanoindentation shows that after a nominal dose of ~3.8–4.0 dpa at ~400°C, PM-HIP 316 L stainless steel has lower hardness than its cast counterpart, consistent with the aforementioned tensile characteristics.
3. TEM microstructural characterization of SA508 irradiated to ~1 dpa at ~384°C–388°C, reveals that although the PM-HIP material nucleates a higher number density of irradiation-induced dislocation loops, their diameters are smaller than in the forged material.
4. APT characterization presents a finer distribution of Ni-Mn-Si nanoclusters in PM-HIP Grade 91 than in its cast counterpart, following 0.99 dpa, 389°C irradiation, despite the PM-HIP having a higher bulk concentration of the clustering species.

Results generally show favorable irradiation performance of PM-HIP alloys, relative to their cast or forged counterparts, as summarized for all alloys studied within the present irradiation campaign in Table 2. Future code qualification efforts for the respective PM-HIP alloys may leverage these data as evidence of the irradiation resilience of PM-HIP materials relative to the already qualified methods of casting or forging. This NSUF campaign may serve as a model for future irradiation and PIE experiments seeking to generate nuclear code qualification data for new fuels and materials, advanced manufacturing methods, or advanced welding and joining technologies. The breadth of NSUF capabilities leveraged herein can also provide a template for designing future NSUF supported programs to evaluate structure–property relationships in irradiated materials and fuels. Finally, all specimens described in this work are available in the NSUF Nuclear Fuels & Materials Library, through which they are openly and competitively available to the community for follow-on research.

Data availability statement

The datasets presented in this study can be found in online repositories. The names of the repository/repositories and accession number(s) can be found below: https://doi.org/10.1016/j.dib.2023.109092.

Author contributions

JW: Conceptualization, Data curation, Funding acquisition, Methodology, Project administration, Supervision, Writing–original draft. DG: Data curation, Formal Analysis, Funding acquisition, Methodology, Project administration, Writing–original draft, Writing–review and editing. CC: Data curation, Formal Analysis, Investigation, Visualization, Writing–review and editing. SB: Data curation, Formal Analysis, Investigation, Visualization, Writing–review and editing. WJ: Data curation, Formal Analysis, Investigation, Visualization, Writing–review and editing. YL: Data curation, Formal Analysis, Investigation, Writing–review and editing. YW: Data curation, Formal Analysis, Investigation, Writing–review and editing. C-HS: Data curation, Formal Analysis, Investigation, Writing–review and editing. DF: Data curation, Formal Analysis, Investigation, Writing–review and editing. BH: Project administration, Resources, Writing–original draft, Writing–review and editing. CK: Project administration, Resources, Writing–review and editing. DG: Conceptualization, Funding acquisition, Resources, Writing–review and editing.

Funding

The author(s) declare financial support was received for the research, authorship, and/or publication of this article. Work at Purdue is supported by the Electric Power Research Institute Agreement 10015819. Nanoindentation, TEM, and APT experiments are conducted at the Microscopy and Characterization Suite, Center for Advanced Energy Studies through the Nuclear Science User Facilities. Irradiation experiments and post-irradiation examination are supported by the US Department of Energy, Office of Nuclear Energy under DOE Idaho Operations Office Contract DE-AC07-05ID14517 as part of Nuclear Science User Facilities Award #CFA-15-8242.

Acknowledgments

In the spirit of this special issue of Frontiers, thank you to the female trailblazers and Sisters in Nuclear who have inspired my onward pursuit of nuclear energy research. –JW. The authors thankful to the project team at Idaho National Laboratory who managed, designed, analyzed, and assembled this experiment,

including Gregory Housley, Cody Hale, Jason Brookman, Katie Anderson, Katelyn Baird, Dave Swank, DC Haggard, and Dave Cottle.

Conflict of interest

Author CC was employed by Westinghouse Electric Company, LLC.

The remaining authors declare that the research was conducted in the absence of any commercial or financial relationships that could be construed as a potential conflict of interest.

Publisher's note

All claims expressed in this article are solely those of the authors and do not necessarily represent those of their affiliated organizations, or those of the publisher, the editors and the reviewers. Any product that may be evaluated in this article, or claim that may be made by its manufacturer, is not guaranteed or endorsed by the publisher.

References

Aguiar, J. A., Jokisaari, A. M., Kerr, M., and Allen Roach, R. (2020). Bringing nuclear materials discovery and qualification into the 21st century. *Nat. Commun.* 11, 2556–2612. doi:10.1038/s41467-020-16406-2

Ahmed, R., Ashraf, A., Elameen, M., Faisal, N. H., El-Sherik, A. M., Elakwah, Y. O., et al. (2014). Single asperity nanoscratch behaviour of HIPed and cast Stellite 6 alloys. *Wear* 312, 70–82. doi:10.1016/j.wear.2014.02.006

Ahmed, R., De Villiers Lovelock, H. L., Davies, S., and Faisal, N. H. (2013). Influence of Re-HIPing on the structure-property relationships of cobalt-based alloys. *Tribol. Int.* 57, 8–21. doi:10.1016/j.triboint.2012.06.025

Atkinson, H., and Davies, S. (2000). Fundamental aspects of hot isostatic pressing: an overview. *Metallurgical Mater. Trans. A* 31A, 2981–3000. doi:10.1007/s11661-000-0078-2

Barros, T. S., Pecly, P. H. R., Pardal, J. M., Gonzaga, A. C., and Tavares, S. S. M. (2022). Comparison between hot rolled and powder metallurgy–hot isostatic pressing (PM-HIP) processed duplex stainless steel UNS S32205. *J. Mater Eng. Perform.* 31, 5504–5510. doi:10.1007/s11665-022-06616-8

Blevins, J., and Yang, G. (2020). Machine learning enabled advanced manufacturing in nuclear engineering applications. *Nucl. Eng. Des.* 367, 110817. doi:10.1016/j.nucengdes.2020.110817

Bonny, G., Terentyev, D., Bakaev, A., Zhurkin, E. E., Hou, M., Van Neck, D., et al. (2013). On the thermal stability of late blooming phases in reactor pressure vessel steels: an atomistic study. *J. Nucl. Mater.* 442, 282–291. doi:10.1016/j.jnucmat.2013.08.018

Bonny, G., Terentyev, D., Zhurkin, E. E., and Malerba, L. (2014). Monte Carlo study of decorated dislocation loops in FeNiMnCu model alloys. *J. Nucl. Mater.* 452, 486–492. doi:10.1016/j.jnucmat.2014.05.051

Brookman, J. (2020). *ECAR 4951 BSU-8242 3 DPA as-run physics analysis (INL/EXT-21-64250-Rev000)*. Idaho Falls, ID (United States). doi:10.2172/1819757

Brookman, J. V. (2018). *ATR physics evaluation for BSU-8242 in the A-6, A-7, and A-8 ATR irradiation positions (INL/RPT-22-67629)*. Idaho: Idaho Falls.

Bullens, A. L., Bautista, E., Jaye, E. H., Vas, N. L., Cain, N. B., Mao, K., et al. (2018). Comparative thermal aging effects on PM-HIP and forged inconel 690. *JOM* 70, 2218–2223. doi:10.1007/s11837-018-2818-z

Chen, T., He, L., Cullison, M. H., Hay, C., Burns, J., Wu, Y., et al. (2020). The correlation between microstructure and nanoindentation property of neutron-irradiated austenitic alloy D9. *Acta Mater* 195, 433–445. doi:10.1016/j.actamat.2020.05.020

Chu, S., and Majumdar, A. (2012). Opportunities and challenges for a sustainable energy future. *Nature* 488, 294–303. doi:10.1038/nature11475

Clement, C., Panuganti, S., Warren, P. H., Zhao, Y., Lu, Y., Wheeler, K., et al. (2022b). Comparing structure-property evolution for PM-HIP and forged alloy 625 irradiated with neutrons to 1 dpa. *Mater. Sci. Eng. A* 857, 144058. doi:10.1016/j.msea.2022.144058

Clement, C., Zhao, Y., Warren, P., Liu, X., Xue, S., Gandy, D. W., et al. (2022a). Comparison of ion irradiation effects in PM-HIP and forged alloy 625. *J. Nucl. Mater.* 558, 153390. doi:10.1016/j.jnucmat.2021.153390

Crawford, D. C., Porter, D. L., Hayes, S. L., Meyer, M. K., Petti, D. A., and Pasamehmetoglu, K. (2007). An approach to fuel development and qualification. *J. Nucl. Mater.* 371, 232–242. doi:10.1016/j.jnucmat.2007.05.029

Davis, K. L., and Hone, L. A. (2020). *NSUF metl wire evaluations for BSU-8242 and GE hitachi-10393 irradiation experiments (INL/EXT-20-58375-Rev0)*. Idaho: Idaho Falls.

De Bellefon, G. M., and Van Duysen, J. C. (2016). Tailoring plasticity of austenitic stainless steels for nuclear applications: review of mechanisms controlling plasticity of austenitic steels below 400 °C. *J. Nucl. Mater.* 475, 168–191. doi:10.1016/j.jnucmat.2016.04.015

Du, C., Jin, S., Fang, Y., Li, J., Hu, S., Yang, T., et al. (2018). Ultrastrong nanocrystalline steel with exceptional thermal stability and radiation tolerance. *Nat. Commun.* 9, 5389. doi:10.1038/s41467-018-07712-x

Everton, S. K., Hirsch, M., Stravroulakis, P., Leach, R. K., and Clare, A. T. (2016). Review of *in-situ* process monitoring and *in-situ* metrology for metal additive manufacturing. *Mater Des.* 95, 431–445. doi:10.1016/j.matdes.2016.01.099

Fujii, K., Fukuya, K., Nakata, N., Hono, K., Nagai, Y., and Hasegawa, M. (2005). Hardening and microstructural evolution in A533B steels under high-dose electron irradiation. *J. Nucl. Mater.* 340, 247–258. doi:10.1016/j.jnucmat.2004.12.008

Gandy, D. W., Shingledecker, J., and Siefert, J. (2012). Overcoming Barriers for Using PM/HIP Technology to Manufacture Large Power Generation Components PM/HIP opens up a new method of manufacturing high pressure-retaining components for use in the power-generation industry. *Adv. Mater. Process.* ASM International 170, 1–8.

Gandy, D. W., Siefert, J., Smith, R., Anderson, P., Lherbier, L., Novotnak, D., et al. (2016). Development of a cobalt-free hard-facing alloy — NitroMaxx-PM for nuclear applications, in: World PM2016.

Gandy, D. W., Stover, C., Bridger, K., and Lawler, S., Small modular reactor vessel manufacture/fabrication using PM-HIP and electron beam welding technologies, materials research proceedings (hot isostatic pressing: HIP'17). 10 (2019) 224–234. doi:10.21741/9781644900031-29

Getto, E. M., Tobie, B., Bautista, E., Bullens, A. L., Kroll, Z. T., Pavel, M. J., et al. (2019). Thermal aging and the Hall–petch relationship of PM-HIP and wrought alloy 625. *JOM* 71, 2837–2845. doi:10.1007/s11837-019-03532-6

Gong, X., Li, R., Sun, M., Ren, Q., Liu, T., and Short, M. P. (2016). Opportunities for the LWR ATF materials development program to contribute to the LBE-cooled ADS materials qualification program. *J. Nucl. Mater.* 482, 218–228. doi:10.1016/j.jnucmat.2016.10.012

Guillen, D. P., Pagan, D. C., Getto, E. M., and Wharry, J. P. (2018). *In situ* tensile study of PM-HIP and wrought 316L stainless steel and inconel 625 alloys with high energy diffraction microscopy. *Mater. Sci. Eng. A* 738, 380–388. doi:10.1016/J.MSEA.2018.09.083

Guillen, D. P., Wharry, J. P., Housley, G., Hale, C. D., Brookman, J., and Gandy, D. W. (2023). Experiment design for the neutron irradiation of PM-HIP alloys for nuclear reactors, *Nucl. Eng. Des.* 402, 112114. doi:10.1016/j.nucengdes.2022.112114

Gurovich, B. A., Kuleshova, E. A., Shtrombakh, Ya.I., Erak, D.Yu., Chernobaeva, A. A., and Zabusov, O. O. (2009). Fine structure behaviour of VVER-1000 RPV materials under irradiation. *J. Nucl. Mater.* 389, 490–496. doi:10.1016/j.jnucmat.2009.02.002

Hale, C. (2021). *BSU-8242 as-run thermal analysis (INL/EXT-21-63578-Rev000)*. Idaho Falls, ID (United States). doi:10.2172/1813571

Hale, C. D. (2018). *BSU-8242 programmatic and safety compliance structural and thermal analysis (INL/RPT-22-67627)*. Idaho: Idaho Falls.

Hamaoka, T., Satoh, Y., and Matsui, H. (2010). One-dimensional motion of self-interstitial atom clusters in A533B steel observed using a high-voltage electron microscope. *J. Nucl. Mater.* 399, 26–31. doi:10.1016/j.jnucmat.2009.12.014

Hensley, C., Sisco, K., Beauchamp, S., Godfrey, A., Rezayat, H., McFalls, T., et al. (2021). Qualification pathways for additively manufactured components for nuclear applications. *J. Nucl. Mater.* 548, 152846. doi:10.1016/j.jnucmat.2021.152846

Hyde, J. M., Marquis, E. A., Wilford, K. B., and Williams, T. J. (2011). A sensitivity analysis of the maximum separation method for the characterisation of solute clusters. *Ultramicroscopy* 111, 440–447. doi:10.1016/j.ultramic.2010.12.015

Jiang, W., Zhao, Y., Lu, Y., Wu, Y., Frazer, D., Guillen, D. P., et al. (2023). Comparison of PM-HIP to forged SA508 pressure vessel steel under high-dose neutron irradiation. Available at: http://arxiv.org/abs/2311.11548.

Jiao, Z., and Was, G. S. (2010). The role of irradiated microstructure in the localized deformation of austenitic stainless steels. *J. Nucl. Mater.* 407, 34–43. doi:10.1016/j.jnucmat.2010.07.006

Kautz, E. J., Hagen, A. R., Johns, J. M., and Burkes, D. E. (2019). A machine learning approach to thermal conductivity modeling: a case study on irradiated uranium-

molybdenum nuclear fuels. *Comput. Mater Sci.* 161, 107–118. doi:10.1016/j.commatsci.2019.01.044

Kočık, J., Keilová, E., Čižek, J., and Procházka, I. (2002). TEM and PAS study of neutron irradiated VVER-type RPV steels. *J. Nucl. Mater.* 303, 52–64. doi:10.1016/S0022-3115(02)00800-0

Kuleshova, E. A., Gurovich, B. A., Shtrombakh, Ya.I., Erak, D.Yu., and Lavrenchuk, O. V. (2002). Comparison of microstructural features of radiation embrittlement of VVER-440 and VVER-1000 reactor pressure vessel steels. *J. Nucl. Mater.* 300, 127–140. doi:10.1016/S0022-3115(01)00752-8

Lind, A., and Bergenlid, U. (2000). Mechanical properties of hot isostatic pressed type 316LN steel after irradiation. *J. Nucl. Mater.* 58–59, 451–454. doi:10.1016/s0022-3115(00)00084-2

Lind, A., and Bergenlid, U. (2001). Mechanical properties of hot isostatic pressed type 316LN steel after irradiation to 2.5 dpa. *Fusion Eng. Des.* 58–59, 713–717. doi:10.1016/S0920-3796(01)00541-5

Mao, K., Wang, H., Wu, Y., Tomar, V., and Wharry, J. P. (2018). Microstructure-property relationship for AISI 304/308L stainless steel laser weldment. *Mater. Sci. Eng. A* 721, 234–243. doi:10.1016/j.msea.2018.02.092

Mao, K. S., Wu, Y., Sun, C., Perez, E., and Wharry, J. P. (2018). Laser weld-induced formation of amorphous Mn–Si precipitate in 304 stainless steel. *Mater. (Oxf)* 3, 174–177. doi:10.1016/j.mtla.2018.08.012

Mao, K. S., French, A. J., Liu, X., Wu, Y., Giannuzzi, L. A., Sun, C., et al. (2021). Microstructure and microchemistry of laser welds of irradiated austenitic steels. *Mater Des.* 206, 109764. doi:10.1016/j.matdes.2021.109764

Mao, K. S., Sun, C., Shiau, C.-H., Yano, K. H., Freyer, P. D., El-Azab, A. A., et al. (2020). Role of cavities on deformation-induced martensitic transformation pathways in a laser-welded, neutron irradiated austenitic stainless steel. *Scr Mater* 178, 1–6. doi:10.1016/j.scriptamat.2019.10.037

Mathew, M. D. (2022). Nuclear energy: a pathway towards mitigation of global warming. *Prog. Nucl. Energy* 143, 104080. doi:10.1016/j.pnucene.2021.104080

Maussner, G., Scharf, L., Langer, R., and Gurovich, B. (1999). Microstructure alterations in the base material, heat affected zone and weld metal of a 440-VVER-reactor pressure vessel caused by high fluence irradiation during long term operation; material: 15 Ch2MFA ≈0.15 C–2.5 Cr–0.7 Mo–0.3 V. *Nucl. Eng. Des.* 193, 359–376. doi:10.1016/S0029-5493(99)00192-2

McMurtrey, M. D., Was, G. S., Patrick, L., and Farkas, D. (2011). Relationship between localized strain and irradiation assisted stress corrosion cracking in an austenitic alloy. *Mater. Sci. Eng. A* 528, 3730–3740. doi:10.1016/j.msea.2011.01.073

Meslin, E., Lambrecht, M., Hernández-Mayoral, M., Bergner, F., Malerba, L., Pareige, P., et al. (2010). Characterization of neutron-irradiated ferritic model alloys and a RPV steel from combined APT, SANS, TEM and PAS analyses. *J. Nucl. Mater.* 406, 73–83. doi:10.1016/j.jnucmat.2009.12.021

Metals, and Ceramics Information Center Report No (1977). *MCIC-77-34 (november 1977)*. Columbus, Ohio.

Moorehead, M., Nelaturu, P., Elbakhshwan, M., Parkin, C., Zhang, C., Sridharan, K., et al. (2021). High-throughput ion irradiation of additively manufactured compositionally complex alloys. *J. Nucl. Mater.* 547, 152782. doi:10.1016/j.jnucmat.2021.152782

Morgan, D., Pilania, G., Couet, A., Uberuaga, B. P., Sun, C., and Li, J. (2022). Machine learning in nuclear materials research. *Curr. Opin. Solid State Mater Sci.* 26, 100975. doi:10.1016/j.cossms.2021.100975

Morrison, A., Sulley, J., Carpenter, C., Borradaile, B., Jones, G., and Warner, T. (2019). HIPed low alloy steel for nuclear pressure vessel applications – material property and microstructural assessment. *Proc. Int. Conf. Nucl. Eng. (ICONE).* 27, 1021. doi:10.1299/jsmeicone.2019.27.1021

Motta, A. T. (1997). *Amorphization of intermetallic compounds under irradiation-A review*.

Murty, K. L., and Charit, I. (2008). Structural materials for Gen-IV nuclear reactors: challenges and opportunities. *J. Nucl. Mater.* 383, 189–195. doi:10.1016/j.jnucmat.2008.08.044

Odette, G. R., and Hoelzer, D. T. (2010). Irradiation-tolerant nanostructured ferritic alloys: transforming helium from a liability to an asset. *JOM* 62, 84–92. doi:10.1007/s11837-010-0144-1

Oliver, W. C., and Pharr, G. M. (2004). Measurement of hardness and elastic modulus by instrumented indentation: advances in understanding and refinements to methodology. *J. Mater Res.* 19, 3–20. doi:10.1557/jmr.2004.19.1.3

Olson, G. B., and Kuehmann, C. J. (2014). Materials genomics: from CALPHAD to flight. *Scr Mater* 70, 25–30. doi:10.1016/j.scriptamat.2013.08.032

Parish, C. M., Field, K. G., Certain, A. G., and Wharry, J. P. (2015). Application of STEM characterization for investigating radiation effects in BCC Fe-based alloys. *J. Mater Res.* 30, 1275–1289. doi:10.1557/jmr.2015.32

Patki, P. V., Wu, Y. Q., and Wharry, J. P. (2020). Effects of proton irradiation on microstructure and mechanical properties of nanocrystalline Cu–10at%Ta alloy. *Mater. (Oxf).* 9, 100597. doi:10.1016/j.mtla.2020.100597

Petti, D., Maki, J., Hunn, J., Pappano, P., Barnes, C., Saurwein, J., et al. (2010). The DOE advanced gas reactor fuel development and qualification program. *JOM* 62, 62–66. doi:10.1007/s11837-010-0140-5

Rao, G. A., Kumar, M., Srinivas, M., and Sarma, D. S. (2003). Effect of standard heat treatment on the microstructure and mechanical properties of hot isostatically pressed superalloy inconel 718. *Mater. Sci. Eng. A* 355, 114–125. doi:10.1016/S0921-5093(03)00079-0

Rodchenkov, B. S., Prokhorov, V. I., Makarov, O. Y., Shamardin, V. K., Kalinin, G. M., Strebkov, Y. S., et al. (2000). Effect of ITER components manufacturing cycle on the irradiation behaviour of 316L(N)-IG steel. *J. Nucl. Mater.* 283–287, 1166–1170. doi:10.1016/s0022-3115(00)00319-6

Sailor, W. C., Bodansky, D., Braun, C., Fetter, S., and van der Zwaan, B. (2000). A nuclear solution to climate change? *Science* 288, 1177–1178. doi:10.1126/science.288.5469.1177

Sen, A., Bachhav, M., Vurpillot, F., Mann, J. M., Morgan, P. K., Prusnick, T. A., et al. (2021). Influence of field conditions on quantitative analysis of single crystal thorium dioxide by atom probe tomography. *Ultramicroscopy* 220, 113167. doi:10.1016/j.ultramic.2020.113167

Shulga, A. V., Effect of heat treatment on carbon behaviour in the HIPed products of the type EP962P Ni-based superalloys, in: Euro PM 2012 - Hot Isostatic Pressing 3, 2012: pp. 1–6.

Shulga, A. V. (2013). A comparative study of the mechanical properties and the behavior of carbon and boron in stainless steel cladding tubes fabricated by PM HIP and traditional technologies. *J. Nucl. Mater.* 434, 133–140. doi:10.1016/j.jnucmat.2012.11.008

Shulga, A. V. (2014). Effect of thermal aging on the mechanical properties of austenitic and ferritic/martensitic stainless steels manufactured by PM HIP and traditional technologies. 1–6. Euro PM 2014 congress and exhibition. Proceedings, Available at: http://www.scopus.com/inward/record.url?eid=2-s2.0-84959042666&partnerID=tZOtx3y1.

Stach, E., DeCost, B., Kusne, A. G., Hattrick-Simpers, J., Brown, K. A., Reyes, K. G., et al. (2021). Autonomous experimentation systems for materials development: a community perspective. *Matter* 4, 2702–2726. doi:10.1016/j.matt.2021.06.036

Sun, C., Wang, Y., McMurtrey, M. D., Jerred, N. D., Liou, F., and Li, J. (2021). Additive manufacturing for energy: a review. *Appl. Energy* 282, 116041. doi:10.1016/j.apenergy.2020.116041

Swenson, M. J., and Wharry, J. P. (2015). The comparison of microstructure and nanocluster evolution in proton and neutron irradiated Fe–9%Cr ODS steel to 3 dpa at 500 °C. *J. Nucl. Mater.* 467, 97–112. doi:10.1016/j.jnucmat.2015.09.022

Swenson, M. J., and Wharry, J. P. (2016). Collected data set size considerations for atom probe cluster analysis. *Microsc. Microanal.* 22, 690–691. doi:10.1017/S143192761600430X

Terrani, K. A., Capps, N. A., Kerr, M. J., Back, C. A., Nelson, A. T., Wirth, B. D., et al. (2020). Accelerating nuclear fuel development and qualification: modeling and simulation integrated with separate-effects testing. *J. Nucl. Mater.* 539, 152267. doi:10.1016/j.jnucmat.2020.152267

van Osch, E. V., Horsten, M. G., de Vries, M. I., van Witzenburg, W., Conrad, R., Sordon, G., et al. (1996). Low temperature irradiation experiments and material testing in Petten. *J. Nucl. Mater.* 233–237, 1541–1546. doi:10.1016/s0022-3115(96)00134-1

Vaumousse, D., Cerezo, A., and Warren, P. J. (2003). A procedure for quantification of precipitate microstructures from three-dimensional atom probe data. *Ultramicroscopy* 95, 215–221. doi:10.1016/S0304-3991(02)00319-4

West, E. A., McMurtrey, M. D., Jiao, Z., and Was, G. S. (2012). Role of localized deformation in irradiation-assisted stress corrosion cracking initiation. *Metall. Mater Trans. A Phys. Metall. Mater Sci.* 43, 136–146. doi:10.1007/s11661-011-0826-5

Wharry, J. P., Clement, C. D., Zhao, Y., Baird, K., Frazer, D., Burns, J., et al. (2023). Mechanical testing data from neutron irradiations of PM-HIP and conventionally manufactured nuclear structural alloys. *Data Brief.* 48, 109092. doi:10.1016/j.dib.2023.109092

Wharry, J. P., and Mao, K. S. (2020). The role of irradiation on deformation-induced martensitic phase transformations in face-centered cubic alloys. *J. Mater Res.* 35, 1660–1671. doi:10.1557/jmr.2020.80

Williams, C. A., Haley, D., Marquis, E. A., Smith, G. D. W., and Moody, M. P. (2013). Defining clusters in APT reconstructions of ODS steels. *Ultramicroscopy* 132, 271–278. doi:10.1016/j.ultramic.2012.12.011

Yu, H., Ahmed, R., Villiers Lovelock de, H., and Davies, H., Influence of manufacturing process and alloying element content on the tribomechanical properties of cobalt-based alloys, *J. Tribol. Trans. ASME)*. 131 (2009) 011601, 1-011601.12. doi:10.1115/1.2991122

Yu, K. Y., Sun, C., Chen, Y., Liu, Y., Wang, H., Kirk, M. A., et al. (2013). Superior tolerance of Ag/Ni multilayers against Kr ion irradiation: an *in situ* study. *Philos. Mag.* 93, 3547–3562. doi:10.1080/14786435.2013.815378

Zain-ul-abdein, M., and Nélias, D. (2016). Effect of coherent and incoherent precipitates upon the stress and strain fields of 6xxx aluminium alloys: a numerical analysis. *Int. J. Mech. Mater. Des.* 12, 255–271. doi:10.1007/s10999-015-9298-x

Zhang, X., Hattar, K., Chen, Y., Shao, L., Li, J., Sun, C., et al. (2018). Radiation damage in nanostructured materials. *Prog. Mater Sci.* 96, 217–321. doi:10.1016/j.pmatsci.2018.03.002